

De novo reconstitution reveals the proteins required for skeletal muscle voltage-induced Ca^{2+} release

Stefano Perna^a, Manuela Lavorato^b, and Kurt G. Beam^{a,1}

^aDepartment of Physiology and Biophysics, Anschutz Medical Campus, University of Colorado, Aurora, CO 80045; and ^bDepartment of Cell and Developmental Biology, Perelman School of Medicine, University of Pennsylvania, Philadelphia, PA 19104

Contributed by Kurt G. Beam, November 14, 2017 (sent for review September 20, 2017; reviewed by Christopher A. Ahern and Mark T. Nelson)

Skeletal muscle contraction is triggered by Ca^{2+} release from the sarcoplasmic reticulum (SR) in response to plasma membrane (PM) excitation. In vertebrates, this depends on activation of the RyR1 Ca^{2+} pore in the SR, under control of conformational changes of $\text{Ca}_v1.1$, located ~ 12 nm away in the PM. Over the last ~ 30 y, gene knockouts have revealed that $\text{Ca}_v1.1/\text{RyR1}$ coupling requires additional proteins, but leave open the possibility that currently untested proteins are also necessary. Here, we demonstrate the reconstitution of conformational coupling in tsA201 cells by expression of $\text{Ca}_v1.1$, $\beta 1a$, Stac3, RyR1, and junctophilin2. As in muscle, depolarization evokes Ca^{2+} transients independent of external Ca^{2+} entry and having amplitude with a saturating dependence on voltage. Moreover, freeze-fracture electron microscopy indicates that the five identified proteins are sufficient to establish physical links between $\text{Ca}_v1.1$ and RyR1. Thus, these proteins constitute the key elements essential for excitation–contraction coupling in skeletal muscle.

calcium signaling | excitation–contraction coupling | $\text{Ca}_v1.1$ | RyR1 | junctophilin

In vertebrate skeletal muscle, the coupling of excitation to contraction (EC coupling) functions under demanding conditions, including high firing rates, hypoxia, and metabolic acidosis. A key step in EC coupling is the transduction of electrical excitation into intracellular release of calcium, which in turn triggers muscle contraction. This transduction occurs at triad junctions in which surface membrane invaginations, the transverse tubules, are flanked on two sides by the sarcoplasmic reticulum (SR): Depolarization of the transverse tubules elicits Ca^{2+} release from the SR. Experiments on muscle cells, which are genetically null for specific triadic proteins (1, 2), have revealed that $\text{Ca}_v1.1$ is the protein which responds to transverse tubular voltage changes and that RyR1 is the channel that gates SR Ca^{2+} release, a process that can occur in skeletal muscle without the entry of extracellular calcium (3). More recent work with gene-deletion models showed that functional and structural interactions between $\text{Ca}_v1.1$ and RyR1 in muscle depend upon the simultaneous presence of at least two additional proteins, the $\beta 1a$ auxiliary subunit (4, 5) of $\text{Ca}_v1.1$ and the Stac3 adaptor protein (6–9). However, these experiments have not been able to establish the mechanism of the $\text{Ca}_v1.1$ –RyR1 interaction or whether currently unidentified proteins are also essential. This latter possibility is given added emphasis by the fact that, until recently, Stac3 was not known to be a triadic protein (6, 8).

Because they must operate under stringent conditions, triad junctions contain a large complex of proteins, only some of which are directly essential for the transduction process. This complexity, together with the fact that SR Ca^{2+} release depends on the interaction between two polarized membrane systems, has greatly hindered the use of reductionist approaches for defining the molecular mechanism of EC coupling Ca^{2+} release. These difficulties are illustrated by a prior attempt to recapitulate such Ca^{2+} release by means of heterologous expression, which has been a primary method for identifying the sets of proteins required for the function of specific ion channels. In that earlier work, an attempt was made to reconstitute EC coupling Ca^{2+} release in CHO cells by coexpressing a Ca_v1 construct, auxiliary Ca_v subunits, and RyR1 (10).

This approach encountered two major problems. The first was that high-level expression of $\text{Ca}_v1.1$ was unobtainable, forcing the authors to use a chimeric construct containing $>90\%$ $\text{Ca}_v1.2$ sequence. The second problem was that endoplasmic reticulum (ER)–plasma membrane (PM) junctions did not form in the transfected CHO cells. As a result, these cells produced only very slow cytoplasmic Ca^{2+} increases dependent upon extracellular Ca^{2+} entry.

Here, we have overcome these problems by (i) obtaining robust $\text{Ca}_v1.1$ expression in tsA201 cells by coexpression of Stac3, and (ii) demonstrating that, in these cells, junctophilin2 (JP2) promotes ER–PM junctions which contain RyR1 and are morphologically similar to SR–PM junctions in muscle cells. These have allowed us to demonstrate that $\text{Ca}_v1.1$, $\beta 1a$, Stac3, RyR1, and JP2 are sufficient to induce ER–PM junctions in which $\text{Ca}_v1.1$ and RyR1 interact with one another both functionally, producing intracellular Ca^{2+} release resembling that in skeletal muscle, and structurally, causing $\text{Ca}_v1.1$ to be arranged into tetrads indicative of physical links to RyR1.

Results

JP2 Promotes ER–PM Junctions. As a first step toward identifying proteins sufficient to enable functional and structural interactions between $\text{Ca}_v1.1$ and RyR1, it was important (i) to be able to identify the minority of cells transiently expressing multiple cDNA constructs, and (ii) to establish the conditions that would cause the formation of ER–PM junctions. Taking both into account, we determined whether JP2 tagged on its amino terminus with YFP (YFP–JP2) would produce ER–PM junctions identifiable by yellow fluorescence. Previous work had shown that the junctophilin family of proteins has a short, C-terminal segment

Significance

Excitation–contraction coupling (ECC) in vertebrate skeletal muscle depends upon specialized junctions at which $\text{Ca}_v1.1$, a voltage-gated channel in the plasma membrane, interacts with RyR1, a calcium release channel in the sarcoplasmic reticulum. Because calcium flux via $\text{Ca}_v1.1$ is unnecessary for ECC, $\text{Ca}_v1.1$ is thought to “conformationally couple” to RyR1. Studies of muscle cells with gene knockouts have shown that additional, junctional proteins are also necessary, but are unable to reveal whether or not these complete the set of required proteins. Here, we show that conformational coupling can be conferred upon tsA201 cells by expressing five junctional proteins ($\text{Ca}_v1.1$, RyR1, $\beta 1a$, Stac3, and junctophilin2), thus establishing a minimum set of proteins supporting $\text{Ca}_v1.1$ –RyR1 conformational coupling in skeletal muscle.

Author contributions: S.P. and K.G.B. designed research; S.P. and M.L. performed research; S.P. and K.G.B. analyzed data; and S.P. and K.G.B. wrote the paper.

Reviewers: C.A.A., University of Iowa; and M.T.N., University of Vermont, College of Medicine.

The authors declare no conflict of interest.

Published under the PNAS license.

¹To whom correspondence should be addressed. Email: Kurt.Beam@ucdenver.edu.

This article contains supporting information online at www.pnas.org/lookup/suppl/doi:10.1073/pnas.1716461115/-DCSupplemental.

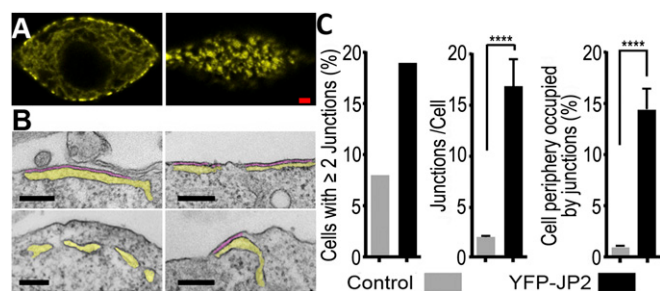


Fig. 1. Expression of YFP-JP2 induces the formation of extensive ER-PM junctions in tsA201 cells. (A) Midlevel (Left) and surface (Right) confocal sections of a transiently transfected tsA201 cell reveal clustering of YFP-JP2 at the cell periphery. (Scale bar, 2 μm .) (B) Thin-section electron micrographs reveal that the peripherally clustered YFP-JP2 likely corresponds to ER-PM junctions. Representative images are shown of cells transfected with YFP-JP2 (Upper) or nontransfected cells (Lower) with yellow and purple shading to indicate ER lumen and junctional gap, respectively. (Scale bars, 200 nm.) (C) Quantitative morphometry reveals that transfection increased the fraction of cells displaying ER-PM junctions, the average length of the junctions, and the percentage of the cellular periphery occupied by those junctions. Transfection efficiency was $\sim 20\%$, and the analysis of junctions per cell and percentage of cellular periphery occupied were carried out for cells with two or more junctions (Table S1). Based on Welch's adjusted *t* test, the bracketed values were significantly different. *****P* < 0.0001.

anchored in the ER and repeated "MORN" motifs which are nearer to the N terminus and associate with the PM, thereby causing the junctional association of these two membrane systems (11). Of the two junctophilin isoforms expressed in skeletal muscle, we selected JP2 because it is expressed earlier during development than JP1 and is able to support the EC coupling of limb muscle in the absence of JP1 (12). As shown in Fig. 1A, tsA201 cells expressing YFP-JP2 displayed prominent, ~ 0.5 - to 2.0 - μm yellow patches of fluorescence associated with the surface. Representative thin-section electron micrographs (Fig. 1B) provided strong evidence that these patches correspond to ER-PM junctions, which are numerous in cells expressing YFP-JP2 and relatively rare in nontransfected cells (Fig. 1C and Table S1). Thus, the fluorescent patches at the periphery of cells transfected

with tagged JP2 appear to provide a useful indicator for likely sites of ER-PM junctions.

Ca_v1.1 Traffics to JP2-Induced Junctions. Having found that transfection with JP2 effectively induces the formation of ER-PM junctions, we next tested whether these junctions shared properties with the SR-PM junctions found in muscle cells. One of these properties is that Ca_v1.1 can traffic to SR-PM junctions in the absence of RyR1, since junctions containing Ca_v1.1 are present in "dyspedic" muscle cells genetically null for RyR1 (13). Thus, we determined whether Ca_v1.1 targeted to junctions in tsA201 cells which lack RyR1. Previously, it was shown that in tsA201 cells transfected with YFP-Ca_v1.1, $\beta 1a$, and $\alpha 2$ - $\delta 1$ only, Ca_v1.1 fails to traffic to the surface, as indicated both by the intracellular retention of yellow fluorescence and the absence of gating charge movements that result when Ca_v1.1 is inserted into the PM (14). By contrast, when CFP-JP2 was also present, there were numerous colocalized fluorescent patches of Ca_v1.1 and JP2 at the periphery (Fig. 2A). Moreover, gating charge movements in such cells (Fig. 2B) demonstrated that Ca_v1.1 had actually been inserted into the PM. Thus, in tsA201 cells expressing JP2, as in muscle, the presence of RyR1 did not seem to be required for Ca_v1.1 to traffic efficiently to the PM-ER junctions. Despite this, the calcium currents were of very small size in these cells (Fig. 2C and D). Thus, we tested the effects of the additional presence of Stac3 because it had been shown to affect Ca_v1.1 expression and function in both muscle and tsA201 cells (7, 9, 14). The additional presence of Stac3 did not alter the colocalization of Ca_v1.1 and JP2 at the cell surface (Fig. 2E) and only slightly increased the magnitude of gating charge movement (Fig. 2F). However, Stac3 caused a very large (~ 30 -fold) increase in the amplitude of the L-type Ca²⁺ current (Fig. 2G), which could not be attributed to the ~ 1.5 -fold increase in the magnitude of charge movement (Table S2). Because Stac3 is of evident importance for the function of Ca_v1.1 in muscle (7, 9), it was one of the constructs used in all of the experiments described below. However, to limit the total number of transfected cDNAs, $\alpha 2$ - $\delta 1$ was omitted because its knockdown by siRNA has minor effects on Ca²⁺ current and EC coupling in skeletal myotubes (15, 16). Similarly, its omission had little effect on Ca²⁺ currents in tsA201 cells (Fig. S1).

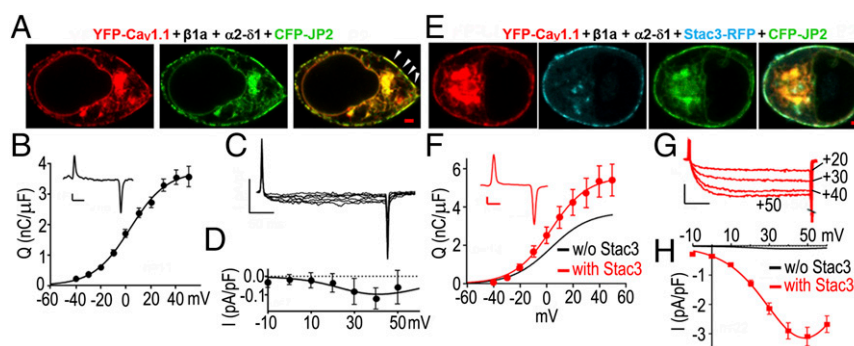


Fig. 2. JP2 causes Ca_v1.1 to insert into discrete domains of the PM, but channel function is minimal without Stac3. (A) Midlevel confocal section of a tsA201 cell transiently transfected with YFP-Ca_v1.1 (red), $\beta 1a$, $\alpha 2$ - $\delta 1$, and CFP-JP2 (green), but not Stac3. A tight colocalization between Ca_v1.1 and JP2 is visible both at the internal (ER) level and at the periphery of the cell where the two proteins are concentrated in discrete foci (some indicated by arrowheads) likely representing ER-PM junctions. (Scale bar, 2 μm .) (B and C) Evidence that the peripherally localized Ca_v1.1, visible in cells like those in A, was inserted into the PM is provided by the presence of gating charge movements (B; representative trace at +40 mV and average ON charge, *n* = 11, as a function of test potential from a holding potential of -80 mV) and small, but detectable, Ca²⁺ currents (C; representative currents for test potentials of -10 to $+50$ mV in 10-mV steps). (D) Average peak currents, *n* = 7, as a function of test potential. (E) Midlevel confocal section of a cell transfected with YFP-Ca_v1.1 (red), $\beta 1a$, $\alpha 2$ - $\delta 1$, Stac3-RFP (cyan), and CFP-JP2 (green): All three tagged proteins colocalize at the cell periphery. (Scale bar, 2 μm .) (F) The additional presence of Stac3 caused only a small increase in the magnitude of gating charge movement (representative trace at +40 mV and average ON charge, *n* = 14, as a function of test potential). (G and H) However, the additional presence of Stac3 caused a very large increase in the amplitude of the Ca²⁺ current: representative currents at the indicated test potentials (G) and average peak current vs. voltage (H) (*n* = 22). The smooth black curves in F and H are replotted from B and D, respectively. Vertical calibration: 1 pA/pF (B, C, and F) or 2 pA/pF (G). Horizontal: 5 ms (B and F) or 50 ms (C and G).

RyR1 Extends from ER to PM. After the demonstration that JP2 caused Ca_v1.1 to traffic to PM junctions with the ER in tsA201 cells, it was next necessary to determine whether RyR1 would also traffic to these junctions. In myotubes, junctional targeting of RyR1 occurs in the absence of Ca_v1.1 (17). In a somewhat similar manner, some RyR1-containing ER was localized near the surface of cells cotransfected with JP2 and not Ca_v1.1, although a large fraction of RyR1 in such cells remained in the cell interior (Fig. S2). By contrast, in cells transfected not only with RyR1 and JP2, but also with Ca_v1.1, β1a, and Stac3, the majority of RyR1 was localized near the surface, where it colocalized with Ca_v1.1 (Fig. 3A), raising the possibility that these two key proteins could functionally and physically interact with one another. Given the resolution limits of fluorescence microscopy, thin-section electron microscopy was used to determine whether electron-dense “feet,” which correspond to the cytoplasmic domain of RyR1 (18), could be observed spanning between the ER and PM. Before this, we created a cell line (“RyR1-stable cells”), in which expression of RyR1 was nearly 100% (Fig. S3) and which thus meant that the number of transiently transfected cDNAs could be reduced by one. These RyR1-stable cells and naïve tsA201 cells were then compared after transient transfection of both cell types with YFP–Ca_v1.1, β1a, Stac3, and JP2. Both the naïve and RyR1-stable cells displayed frequent, extended junctions between the ER and PM (Fig. 3B–D). In the naïve cells, the junctional gaps were relatively uniform and electron lucent (Fig. 3B), consistent with the hypothesis that only JP2, which is a small protein, filled those gaps. On the other hand, electron-dense particles with a semiregular spacing were clearly visible in some of the junctions in the RyR1-stable cells (Fig. 3C and D). These particles closely resembled the foot structures described in skeletal muscle triads (19) and peripheral dyads in myotubes (20).

EC Coupling Ca²⁺ Release Recapitulated. For the measurement of Ca²⁺ transients, we switched from conventional whole-cell clamping to the perforated patch technique (21), which was applied to cells that had been loaded with Fluo-3 AM. The perforated patch had

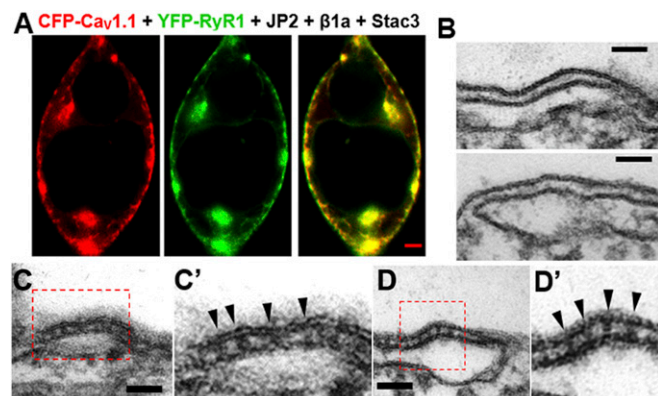


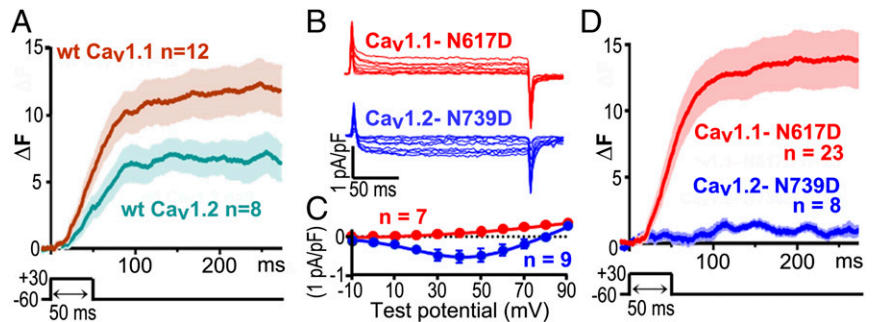
Fig. 3. RyR1 traffics to ER–PM junctions induced by JP2. (A) In cells transiently transfected with CFP–Ca_v1.1 (red), β1a, Stac3, YFP–RyR1 (green), and JP2, the RyR1 fluorescence was colocalized with that of Ca_v1.1, partly in the ER, but mostly at the cell periphery. (Scale bar, 2 μm.) (B–D) Thin-section electron micrographs are shown for naïve tsA201 cells (B) and tsA201 cells stably expressing RyR1 (C and D) obtained after both types of cells were transiently transfected with YFP–Ca_v1.1, β1a, Stac3, and JP2. C' and D' present magnified (2×) views of the indicated areas in C and D. The ER–PM gaps of the junctions in the naïve cells were essentially free of electron-dense material, whereas those in the RyR1-stable cells displayed periodic, electron-dense structures spanning the gap between the ER and PM (arrowheads). These densities resemble in shape and size the feet structures which are observed in triads of skeletal muscle (and dyads of developing skeletal muscle) and which have been attributed to the cytoplasmic domain of RyR1. (Scale bars, 50 nm.)

the disadvantage of increased access resistance, which compromised measurement of membrane currents. However, it had the advantage of minimizing perturbations of intracellular calcium handling, which seemed important given that tsA201 cells lack the adaptations which equip skeletal muscle to efficiently move Ca²⁺ into the ER/SR and to store it there. Even with perforated patch, we found that Ca²⁺ transients were small and that restoration of the ER store was so slow that the second of two responses to identical stimuli was smaller than the first. Thus, it was necessary to compare populations of cells which raised a second issue: A significant fraction of cells not producing a detectable response might simply not have been expressing the entire set of transfected constructs. Because it was not possible to determine whether or not an individual cell was expressing all of the transfected constructs, we calculated average Ca²⁺ transients only from cells in which the responses exceeded a minimum threshold unlikely to have been exceeded in nontransfected cells ($\Delta F \geq 1.5$ in the 200-ms interval after onset of the test pulse).

Fig. 4A compares the average Ca²⁺ transients elicited by a 50-ms depolarization to +30 mV which was applied to RyR1-stable cells transfected with β1a, Stac3–RFP, JP2, and either YFP–Ca_v1.1 (brown trace) or YFP–Ca_v1.2 (teal trace). The transients were quite similar to one another. Furthermore, both Ca_v1.1 and Ca_v1.2 colocalized with RyR1 (Fig. 3A and Fig. S4A, respectively), raising the question of whether these transients resulted from the same underlying mechanism. Previous work had shown that transients triggered by Ca_v1.2, both in native tissue (22) and after expression in dysgenic myotubes (23), depend on entry of external Ca²⁺, and this also appeared to be the case for RyR1-stable cells transfected with YFP–Ca_v1.2, β1a, Stac3–RFP, and JP2. In such cells, cytoplasmic Ca²⁺ remained unchanged during a depolarization to +90 mV, a potential at which Ca²⁺ entry did not occur, and only increased upon subsequent repolarization to –60 mV, which generated an inward tail current (Fig. S4B, which also illustrates the threshold used to include/exclude data for subsequent analysis). To determine whether Ca²⁺ entry was also required for the transients in cells expressing Ca_v1.1, we used two approaches. The first was to measure Ca²⁺ transients in single cells before and after the addition of Cd²⁺ and La³⁺ to the bathing solution. After this addition, inward Ca²⁺ current was effectively eliminated, but Ca²⁺ transients were still present (Fig. S5). As a second approach, we introduced a point mutation into the pore of Ca_v1.1 (N617D) and at the homologous position of Ca_v1.2 (N739D). The N617D mutation eliminates Ca²⁺ permeability of Ca_v1.1 (Fig. 4B and C) without affecting its function in EC coupling (24), and the N739D mutation caused a large reduction of inward Ca²⁺ current via Ca_v1.2 (Fig. 4B and C). Ca²⁺ transients were greatly reduced for Ca_v1.2–N739D (Fig. 4D) compared with WT Ca_v1.2 (Fig. 4A), as expected if the transients for Ca_v1.2 depended on entry of extracellular Ca²⁺. However, the transients were essentially identical for the Ca_v1.1–N617D (Fig. 4D) and WT Ca_v1.1 (Fig. 4A), despite the complete loss of extracellular Ca²⁺ entry. Thus, it seems likely that these transients resulted, as in skeletal muscle, from the conformational activation of RyR1 by Ca_v1.1.

A characteristic feature of EC coupling in skeletal muscle is that Ca²⁺ release increases in magnitude as a sigmoidal function of test potential and saturates for strong depolarizations. Thus, we characterized the voltage dependence of Ca²⁺ release in RyR1-stable cells transfected with YFP–Ca_v1.1–N617D (to prevent possible contributions of Ca²⁺ entry), β1a, Stac3–RFP, and JP2. Due to the weak Ca²⁺ reuptake ability of tsA201 cells, it was not possible to reliably test multiple depolarizations in single cells. Therefore, we measured transients in individual cells in response to a single potential of –30, 0, +30, or +90 mV and included that response as part of the average for that potential if it met the criterion described earlier ($\Delta F \geq 1.5$ within 200 ms of the onset of depolarization). Transients at –30 mV which did not meet this criterion (four cells) were also included in the average if the transient for a subsequent, stronger depolarization did meet it. Average transients obtained in this fashion are

Fig. 4. Five triad-junction proteins are sufficient to produce voltage-gated Ca^{2+} release that does not require entry of extracellular Ca^{2+} . (A) Average cytoplasmic Ca^{2+} transients elicited by a 50-ms depolarization to +30 mV applied, via the perforated patch technique, to RyR-stable cells transiently transfected with $\beta 1\text{a}$, Stac3-RFP, and JP2 together with either YFP-Ca $\text{v}1.1$ (brown line) or YFP-Ca $\text{v}1.2$ (teal line). Data are shown as Fluo-3 fluorescence increase (ΔF) \pm SEM. (B and C) Representative currents and average peak $I-V$ relationships recorded from naïve tsA201 cells transfected with YFP-Ca $\text{v}1.1$ -N617D (red) or Ca $\text{v}1.2$ -N739D, together with $\beta 1\text{a}$, Stac3-RFP, and JP2. Mutation of the conserved IIS6 asparagine to aspartate completely eliminated inward Ca^{2+} current via Ca $\text{v}1.1$ and left only a small inward Ca^{2+} current via Ca $\text{v}1.2$. (D) The average Ca^{2+} transient for Ca $\text{v}1.2$ -N739D (blue) was much smaller than that for WT Ca $\text{v}1.2$, as expected if it depended on the entry of extracellular Ca^{2+} . By contrast, the amplitude of the average transient for YFP-Ca $\text{v}1.1$ -N617D (red) was comparable to that of WT Ca $\text{v}1.1$, consistent with the hypothesis that, as in skeletal muscle, Ca $\text{v}1.1$ activates intracellular Ca^{2+} release without requiring extracellular Ca^{2+} entry. Except for the Ca v constructs used, conditions were identical for the data shown in A and D.



illustrated in Fig. 5A, and their magnitude measured just before repolarization is plotted as a function of test potential in Fig. 5B. Although the number of test potentials was limited, the voltage dependence appeared to be similar to that in skeletal myotubes (25), in regard to both midpoint and slope factor (Table S2).

Interestingly, the fluorescence signals illustrated in Figs. 4 and 5 continued to increase for tens of milliseconds after repolarization to the holding potential. The interpretation of these signals depends upon knowing the flux rates and subcellular localization of the Ca^{2+} release sites, the transport rates and subcellular localization of the Ca^{2+} removal sites, and the concentration and affinities of cellular Ca^{2+} buffers. Although detailed information was lacking, it can be said that the overall rate of removal of Ca^{2+} from the cytoplasm was extremely slow (Fig. S6A). Additionally, the majority of Ca^{2+} release would be expected to occur at the periphery where most of RyR1 is located (e.g., Fig. 3A). Consequently, the rate of fluorescence change at the periphery should be approximately related to the rate of Ca^{2+} release there. On the other hand, the fluorescence change in the cellular interior, where the bulk of the Ca^{2+} indicator is located, would lag because it depends on the diffusion of Ca^{2+} from the release sites, and this diffusion would be slowed by the cellular Ca^{2+} buffers. Evidence that these ideas may be correct was provided by the cell illustrated in Fig. S6B. The fluorescence within the interior continued to increase for ~ 75 ms after repolarization, whereas the fluorescence at the edge of the cell ceased to increase shortly after repolarization. Thus, it appears that repolarization may cause a rapid termination of release at the ER-PM junctions containing Ca $\text{v}1.1$ and RyR1.

Ca $\text{v}1.1$ Physically Links to RyR1. In freeze-fracture replicas of skeletal muscle cells, Ca $\text{v}1.1$ appears as large particles arranged in groups of four (“tetrads”), with each particle aligned with one of the four monomers comprising the RyR1 homotetramer (26). Moreover, the tetradic arrangement depends on the presence of RyR1 (27), thus providing evidence that Ca $\text{v}1.1$ and RyR1 are physically linked to one another in skeletal muscle, either directly or via intervening proteins. To determine whether RyR1 caused Ca $\text{v}1.1$ to be arranged as tetrads in tsA201 cells, we analyzed freeze fractures of RyR1-stable and naïve cells that had been transfected with YFP-Ca $\text{v}1.1$, $\beta 1\text{a}$, Stac3, and CFP-JP2. In both groups of cells, PM domains at sites of junction with the ER (circled in Fig. 6A $_1$ -F $_1$) could be recognized by a slightly raised appearance and the presence of large particles, having the expected size for Ca $\text{v}1.1$ (15, 28). In the RyR1-stable cells, the large particles were spaced fairly evenly and sometimes arrayed as tetrad-like groups containing three or four particles (Fig. 6A-C). Some examples of likely tetrads in the transfected RyR1-stable cells have been overlaid with a ~ 30 - \times 30-nm square (Fig. 6A $_1$ -C $_1$), which corresponds to the outer dimensions of a single tetrad in muscle cells (29, 30). In addition to size, other

features resembling those of tetrads in muscle included the clear separation of the individual particles within each apparent tetrad and the generally similar orientation of the apparent tetrads throughout each junction. By contrast, the large particles in the naïve cells were interspersed with smaller ones, and the large particles appeared to be randomly distributed with occasional clumps (Fig. 6D-F). Of course, randomly distributed particles in the naïve cells would be expected occasionally to be arranged in groups of four, some examples of which are indicated in Fig. 6E $_1$ and F $_1$. However, these differ from the apparent tetrads in the RyR1-stable cells in that they did not have a clear separation between all four particles. Nonetheless, as an independent method for determining whether there was a difference in the prevalence of tetrad-like structures in the naïve and RyR1-stable cells, we asked three investigators to determine the number of tetrads present in unidentified micrographs (Fig. S7). They were 79%, 95%, and 96% accurate in identifying tetrads as preferentially present in the RyR1-stable cells.

Discussion

We have shown here that five proteins, Ca $\text{v}1.1$, $\beta 1\text{a}$, Stac3, JP2, and RyR1, when expressed in tsA201 cells, are sufficient to support Ca^{2+} release which resembles that in skeletal muscle, in that it does not require the entry of external Ca^{2+} and has a saturating dependence on voltage. Moreover, in cells expressing

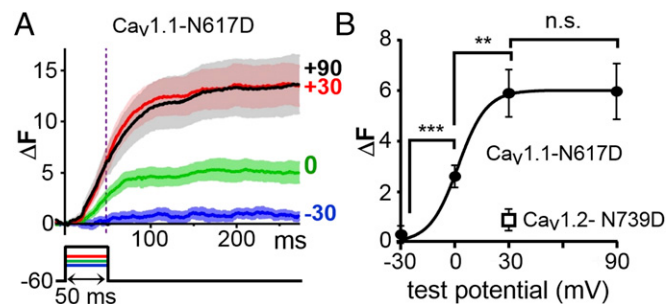


Fig. 5. The voltage dependence of Ca^{2+} release in cells expressing five triad-junction proteins is similar to that of Ca^{2+} release in skeletal muscle. (A) RyR1-stable cells were transiently transfected with YFP-Ca $\text{v}1.1$ -N617D, $\beta 1\text{a}$, Stac3-RFP, and JP2, loaded with Fluo-3 AM, and depolarized to the indicated potentials with the perforated patch technique. Data are presented as mean (solid line) \pm SEM. Number of cells averaged was 10, 13, 24, and 22 for -30, 0, +30, and +90 mV, respectively, is shown. (B) Average ΔF , measured at 48 ms after the onset of depolarization (vertical dotted line in A), as a function of test potential. Based on Welch’s adjusted t test, the bracketed values were statistically different: *** $P = 0.0006$; ** $P = 0.002$; n.s., not significantly different ($P = 0.949$). The data point for Ca $\text{v}1.2$ -N739D was obtained from the eight cells used to generate the average transient in Fig. 4D.

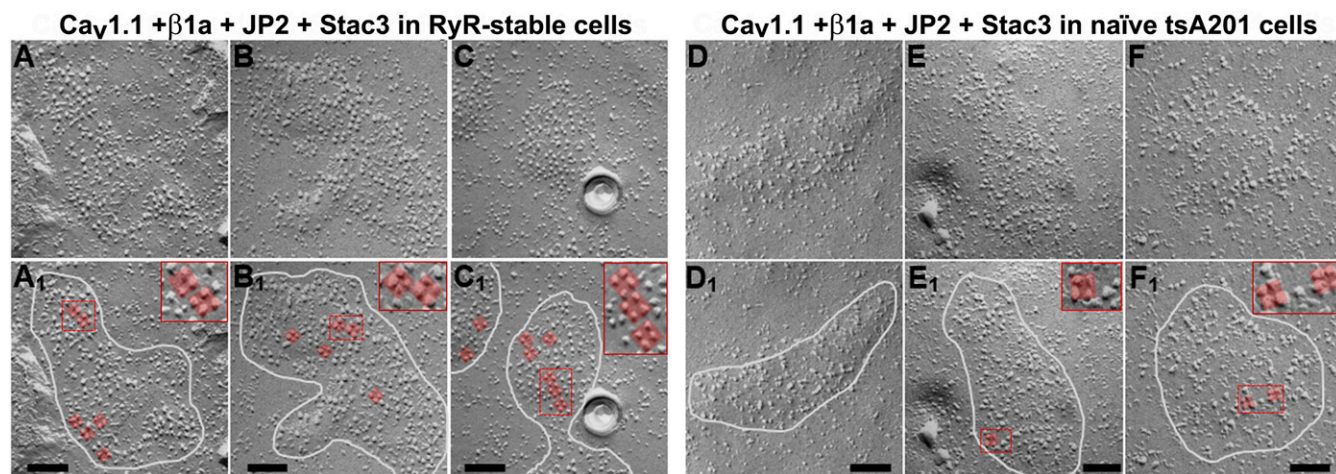


Fig. 6. Intramembranous particles in groups of four (tetrads) indicate that $\text{Ca}_v1.1$ is physically linked to RyR1 in tsA201 cells expressing five triad-junction proteins. Freeze-fracture electron micrographs are shown of RyR1-stable (A–C) and naïve (D–F) tsA201 cells transiently transfected with YFP- $\text{Ca}_v1.1$, $\beta1a$, Stac3, and CFP-JP2. ER-PM junctions in both cell types appear as slightly “domed” structures (encircled by white lines in A₁–F₁), containing clusters of large particles. Some of the large particles in A₁–C₁, E₁, and F₁ have been overlaid with a $\sim 30 \times 30$ -nm red square, and subregions containing some of these squares are magnified 2 \times in *Insets*. A 30×30 -nm square was chosen because tetrads in native muscle cells fit well inside, with one particle at each corner. Such well-fitting groups of particles were evident in junctions of the transfected RyR1-stable cells (A₁–C₁). In some instances, only three particles were present (e.g., A₁, *Inset*), as also occurs in native skeletal muscle, and in other instances the particles appeared to have been deformed during the fracture process. Particles that would fit within a 30×30 -nm square were occasionally found in the transfected, naïve tsA201 (E₁ and F₁), but the fit was generally poorer, and there was a lack of clear separation between individual particles as occurs in skeletal muscle and as was evident for many of the presumptive tetrads in the transfected RyR1-stable cells. (Scale bars, 100 nm.)

these five proteins, it appears likely that $\text{Ca}_v1.1$ and RyR1 are physically linked to one another. Of course, triad junctions in muscle contain many more proteins, some of which interact with one or more of the proteins analyzed in our work. Nonetheless, our results indicate that $\text{Ca}_v1.1$, $\beta1a$, Stac3, JP2, and RyR1 represent fundamental components of the Ca^{2+} release mechanism and are the locus of protein–protein interactions sufficient for functional and structural coupling between $\text{Ca}_v1.1$ and RyR1.

As touched on in the introduction, experiments on myotubes that are null for endogenous $\text{Ca}_v1.1$ (1), RyR1 (2), $\beta1a$ (4, 5), or Stac3 (7, 9) have shown that EC coupling Ca^{2+} release requires the simultaneous presence of all four proteins. Because JP2 would have been present in these null myotubes, these experiments were not informative about whether JP2 is also directly involved in linking $\text{Ca}_v1.1$ to RyR1 or functions only to induce the formation of junctions. In this regard, it would be of interest to determine the extent to which JP1 or the neuronal junctophilins (JP3 and JP4) can substitute for JP2 in producing the $\text{Ca}_v1.1$ –RyR1 coupling in the tsA201 cell system.

Clearly, elucidating the molecular mechanism of EC coupling Ca^{2+} release will require high-resolution structure. In this regard, the structures of the isolated components are likely to be of limited value because previous work has indicated that the absence of RyR1 alters the structures of $\text{Ca}_v1.1$ and $\beta1a$, and that the absence of $\text{Ca}_v1.1$ alters the structure of RyR1. In particular, the absence of RyR1 in muscle cells results in altered gating of $\text{Ca}_v1.1$ (31) and, based on FRET measurements, causes rearrangement of the $\text{Ca}_v1.1$ cytoplasmic domains (32) and likely the N terminus of $\beta1a$ (33). Conversely, the absence of $\text{Ca}_v1.1$ appears to alter RyR1 structure in that resting Ca^{2+} leak via RyR1 is increased in muscle cells lacking $\text{Ca}_v1.1$ (34). Furthermore, the absence of Stac3 significantly affects the function of $\text{Ca}_v1.1$, including its ability to activate RyR1 (7, 9). Thus, it would seem necessary to obtain the structure of $\text{Ca}_v1.1$, $\beta1a$, Stac3, and RyR1 arranged as a working complex. Toward this end, the transfected tsA201 cells provide a system of potentially great value. For this approach to succeed, it will likely be necessary to develop clonal cell lines expressing all five proteins and perhaps also to use cell-sorting techniques. However, these difficulties may be compensated by the greatly simplified protein content of the transfected

tsA201 cells and the ability to dock structures of the assembled complex with those already determined for the large portions of $\text{Ca}_v1.1$, $\beta1a$, and RyR1.

Materials and Methods

Cell Culture and Cell Lines. tsA201 cells were cultured in high-glucose DMEM (Mediatech Inc.) supplemented with 10% (vol/vol) FBS (Gemini Bio Products), 2 mM glutamine (Mediatech Inc.), 100 U/mL penicillin (Gemini Bio Products), and 100 $\mu\text{g}/\text{mL}$ streptomycin (Gemini Bio Products) in a humidified incubator with 5% (vol/vol) CO_2 . Cells at $\sim 70\%$ confluence were transfected according to manufacturer’s instructions for 3.5 h by using the jetPRIME reagent (Polyplus-transfection Inc.) containing either 1 $\mu\text{g}/\mu\text{L}$ cDNA (RyR and Ca_v constructs) or 0.5 $\mu\text{g}/\mu\text{L}$ cDNA (all other constructs). The cells were then detached from the dish with 0.05% trypsin EDTA diluted from a 0.25% stock (Gibco) and replated at $\sim 1.5 \times 10^4$ cells per dish in 35-mm culture dishes for electrophysiology or at $\sim 2.5 \times 10^4$ per cm^2 in ECL (Upstate Biotechnology)-coated, glass-bottomed dishes (14-mm microwell diameter; MatTek) for imaging or freeze-fracture. To generate tsA201 cells stably expressing RyR1, the cells were transfected as described with RyR1-pCEP4 and propagated in medium (described above) supplemented with 300 $\mu\text{g}/\text{mL}$ hygromycin B (Invitrogen) for selection. After establishment of a polyclonal culture, the cells were replated at low density (5,000 cells per 35-mm dish) and maintained for 2–3 d until the isolated single cells had expanded into monoclonal colonies of at least 15–20 cells. The cells were then loaded with Fluo-3 AM (Molecular Probes) (see below), and the monoclonal colonies were tested for their response to localized application of 0.5 mM RyR1 agonist 4-chloro-*m*-cresol (Pfaltz & Bauer, Inc.). Three colonies showing high, uniform response were isolated, subcultured, and expanded before freezing. Clone 1 was used for all of the experiments described here (denoted RyR1-stable cells).

Molecular Biology. For expression plasmids, see *SI Materials and Methods*.

Imaging Analysis. Cells were bathed in physiological saline (in mM: 146 NaCl, 5 KCl, 2 CaCl_2 , 1 MgCl_2 , and 10 HEPES, pH 7.4, with NaOH) and optical slices were obtained by using a Zeiss 710 confocal microscope with a $40\times$ (1.3 NA) or $63\times$ (1.4 NA) objective. Fluorescence excitation (Ex) and emission (Em) (nanometers) were DAPI (Ex, 405; Em, 410–585), GFP (Ex, 488; Em, 493–586), CFP (Ex, 440; Em, 454–503 \pm 5), YFP (Ex, 514; Em, 520 \pm 5–596 \pm 23), mCherry (Ex, 543; Em, 578–696), RFP (Ex, 543; Em, 597–745), and Alexa Fluor 568 (Ex, 543; Em, 568–712).

Measurement of Currents and Cytoplasmic Ca^{2+} Transients. All experiments were performed at room temperature ($\sim 25^\circ\text{C}$). Cells were voltage-clamped with either the whole-cell or perforated patch techniques. For whole-cell recording of ionic currents or charge movements, the pipettes had a resistance of $\sim 3\text{ M}\Omega$ when filled with internal solution of (in mM) 140 Cs-aspartate, 10 Cs-EGTA, 5 MgCl_2 , and 10 Hepes (pH 7.4), with CsOH. After entry into whole-cell mode, electronic compensation was used to reduce the effective series resistance to $< 8\text{ M}\Omega$ (time constant $< 500\ \mu\text{s}$). The bath solution contained (in mM) 145 tetraethylammonium (TEA)-Cl, 10 CaCl_2 , and 10 Hepes (pH 7.4, with TEA-OH). For measurement of charge movements, the bath additionally contained 0.1 mM LaCl_3 and 0.5 mM CdCl_2 .

For perforated patch recording (21) of ionic currents or Ca^{2+} transients, the pipette tip was front-filled by immersing it for $\sim 5\text{ s}$ in internal solution consisting of (in mM): 70 Cs-Aspartate, 10 NaCl, 1 CaCl_2 , 1 MgCl_2 , and 10 Hepes (pH 7.2), with CsOH. The pipette was then back-filled with a 100-fold dilution (in the same solution) of amphotericin stock solution: 20 mg/mL amphotericin (APExBio Technology LLC) and 0.5% (wt/vol) pluronic in DMSO. After giga-seal formation ($\geq 2\text{ G}\Omega$) with a cell, negative pressure on the pipette was released, and cell recording began after access resistance had fallen to $\leq 20\text{ M}\Omega$. The bath contained (in mM): 137 NaCl, 5.6 KCl, 2.6 CaCl_2 , 1.2 MgCl_2 , 10 glucose, and 10 Hepes (pH 7.4), with NaOH.

Depolarizing test steps were applied from a holding potential of -60 mV , unless otherwise noted. Linear leak and capacity currents were corrected by $-P/4$ (whole-cell) or $-P/3$ (perforated patch) subtraction. Signals were analog filtered 1–2 or 5 kHz for ionic currents and charge movements, respectively, and sampled at 20 kHz.

For measurement of cytoplasmic Ca^{2+} transients, cells were loaded for 20 min at 37°C with Fluo-3 AM added to the medium (3.5 μM Fluo-3 AM, 0.035% pluronic, and 0.35% DMSO). The cells were then washed and clamped with the perforated patch technique (see above), with candidate cells selected on the basis of red fluorescence arising from Stac3-tagRFP. A fluorometer apparatus (Biomedical Instrumentation Group, University of

Pennsylvania) equipped with fluorescein optics was used to measure changes in Fluo-3 fluorescence (ΔF) from baseline, in response to 50-ms depolarizations. The baseline was taken as the average fluorescence in the 2- to 4-ms interval immediately preceding the test depolarization.

Electron Microscopy. See *SI Materials and Methods* for sample preparation. To quantify ER-PM junctions, all cells displaying two or more junctions (“positive cells”) were identified in random areas of microscope grids. The fraction of all cells that were positive was recorded, and each positive cell was subsequently analyzed with ImageJ (National Institutes of Health) to determine the lengths of all of the junctions within the cell and the length of the cell perimeter. The percentage of cell perimeter occupied by junctions was calculated by dividing the total junction length by the perimeter for each positive cell, while average junctional length, maximum length, and minimum length were determined from all junctions imaged in the positive cells.

Quantification and Statistical Analysis. Statistical parameters including the exact value of n , dispersion and precision measures (mean \pm SEM), and statistical significance are reported in the figures and figure legends. Data were judged to be statistically significant when $P < 0.05$ by Welch’s adjusted unpaired t test. In figures, asterisks denote statistical significance as calculated by Student’s t test (*, $P < 0.05$; **, $P < 0.01$; ***, $P < 0.001$; ****, $P < 0.0001$). GraphPad Prism 6 software was used for constructing data plots, curve fitting, and statistical analysis.

ACKNOWLEDGMENTS. We thank Drs. Alex Polster, Symeon Papadopoulos, and Eric Olson for providing cDNA constructs; Rock Levinson, William Sather, and John Bankston for counting tetrads; Catherine Proenza for commenting on the manuscript; and Clara Franzini-Armstrong for providing use of the freeze-fracture machine. This work was supported by NIH Grants AR070298 and AR052354; and Muscular Dystrophy Association Grant 277475 (to K.G.B.).

1. Tanabe T, Beam KG, Powell JA, Numa S (1988) Restoration of excitation-contraction coupling and slow calcium current in dysgenic muscle by dihydropyridine receptor complementary DNA. *Nature* 336:134–139.
2. Takeshima H, et al. (1994) Excitation-contraction uncoupling and muscular degeneration in mice lacking functional skeletal muscle ryanodine-receptor gene. *Nature* 369:556–559.
3. Armstrong CM, Bezanilla FM, Horowicz P (1972) Twitches in the presence of ethylene glycol bis-(aminoethyl ether)- N,N' -tetracetic acid. *Biochim Biophys Acta* 267:605–608.
4. Beurg M, et al. (1999) Involvement of the carboxy-terminus region of the dihydropyridine receptor beta1a subunit in excitation-contraction coupling of skeletal muscle. *Biophys J* 77:2953–2967.
5. Schredelseker J, Dayal A, Schwerte T, Franzini-Armstrong C, Grabner M (2009) Proper restoration of excitation-contraction coupling in the dihydropyridine receptor beta1-null zebrafish relaxed is an exclusive function of the beta1a subunit. *J Biol Chem* 284:1242–1251.
6. Horstick EJ, et al. (2013) Stac3 is a component of the excitation-contraction coupling machinery and mutated in Native American myopathy. *Nat Commun* 4:1952.
7. Linsley JW, et al. (2017) Congenital myopathy results from misregulation of a muscle Ca^{2+} channel by mutant Stac3. *Proc Natl Acad Sci USA* 114:E228–E236.
8. Nelson BR, et al. (2013) Skeletal muscle-specific T-tubule protein STAC3 mediates voltage-induced Ca^{2+} release and contractility. *Proc Natl Acad Sci USA* 110:11881–11886.
9. Polster A, Nelson BR, Olson EN, Beam KG (2016) Stac3 has a direct role in skeletal muscle-type excitation-contraction coupling that is disrupted by a myopathy-causing mutation. *Proc Natl Acad Sci USA* 113:10986–10991.
10. Suda N, et al. (1997) Ca^{2+} -induced Ca^{2+} release in Chinese hamster ovary (CHO) cells co-expressing dihydropyridine and ryanodine receptors. *J Gen Physiol* 109:619–631.
11. Takeshima H, Komazaki S, Nishi M, Iino M, Kangawa K (2000) Junctophilins: A novel family of junctional membrane complex proteins. *Mol Cell* 6:11–22.
12. Ito K, et al. (2001) Deficiency of triad junction and contraction in mutant skeletal muscle lacking junctophilin type 1. *J Cell Biol* 154:1059–1067.
13. Takekura H, Franzini-Armstrong C (1999) Correct targeting of dihydropyridine receptors and triadin in dyspedic mouse skeletal muscle in vivo. *Dev Dyn* 214:372–380.
14. Polster A, Perali S, Bichraoui H, Beam KG (2015) Stac adaptor proteins regulate trafficking and function of muscle and neuronal L-type Ca^{2+} channels. *Proc Natl Acad Sci USA* 112:602–606.
15. Gach MP, et al. (2008) Alpha2delta1 dihydropyridine receptor subunit is a critical element for excitation-coupled calcium entry but not for formation of tetrads in skeletal myotubes. *Biophys J* 94:3023–3034.
16. Obermair GJ, et al. (2005) The Ca^{2+} channel alpha2delta-1 subunit determines Ca^{2+} current kinetics in skeletal muscle but not targeting of alpha1S or excitation-contraction coupling. *J Biol Chem* 280:2229–2237.
17. Franzini-Armstrong C, Pincon-Raymond M, Rieger F (1991) Muscle fibers from dysgenic mouse in vivo lack a surface component of peripheral couplings. *Dev Biol* 146:364–376.
18. Kawamoto RM, Brunschwig JP, Kim KC, Caswell AH (1986) Isolation, characterization, and localization of the spanning protein from skeletal muscle triads. *J Cell Biol* 103:1405–1414.
19. Franzini-Armstrong C (1970) STUDIES OF THE TRIAD: I. Structure of the junction in frog twitch fibers. *J Cell Biol* 47:488–499.
20. Protasi F, et al. (2000) RYR1 and RYR3 have different roles in the assembly of calcium release units of skeletal muscle. *Biophys J* 79:2494–2508.
21. Horn R, Marty A (1988) Muscarinic activation of ionic currents measured by a new whole-cell recording method. *J Gen Physiol* 92:145–159.
22. Nábauer M, Callewaert G, Cleemann L, Morad M (1989) Regulation of calcium release is gated by calcium current, not gating charge, in cardiac myocytes. *Science* 244:800–803.
23. Tanabe T, Mikami A, Numa S, Beam KG (1990) Cardiac-type excitation-contraction coupling in dysgenic skeletal muscle injected with cardiac dihydropyridine receptor cDNA. *Nature* 344:451–453.
24. Dayal A, et al. (2017) The Ca^{2+} influx through the mammalian skeletal muscle dihydropyridine receptor is irrelevant for muscle performance. *Nat Commun* 8:475.
25. García J, Beam KG (1994) Measurement of calcium transients and slow calcium current in myotubes. *J Gen Physiol* 103:107–123.
26. Block BA, Imagawa T, Campbell KP, Franzini-Armstrong C (1988) Structural evidence for direct interaction between the molecular components of the transverse tubule/sarcoplasmic reticulum junction in skeletal muscle. *J Cell Biol* 107:2587–2600.
27. Protasi F, Franzini-Armstrong C, Allen PD (1998) Role of ryanodine receptors in the assembly of calcium release units in skeletal muscle. *J Cell Biol* 140:831–842.
28. Takekura H, et al. (2004) Differential contribution of skeletal and cardiac II-III loop sequences to the assembly of dihydropyridine-receptor arrays in skeletal muscle. *Mol Biol Cell* 15:5408–5419.
29. Franzini-Armstrong C, Kish JW (1995) Alternate disposition of tetrads in peripheral couplings of skeletal muscle. *J Muscle Res Cell Motil* 16:319–324.
30. Paolini C, Protasi F, Franzini-Armstrong C (2004) The relative position of RyR feet and DHPR tetrads in skeletal muscle. *J Mol Biol* 342:145–153.
31. Nakai J, et al. (1996) Enhanced dihydropyridine receptor channel activity in the presence of ryanodine receptor. *Nature* 380:72–75.
32. Polster A, Ohrtman JD, Beam KG, Papadopoulos S (2012) Fluorescence resonance energy transfer (FRET) indicates that association with the type I ryanodine receptor (RyR1) causes reorientation of multiple cytoplasmic domains of the dihydropyridine receptor (DHPR) $\alpha(1S)$ subunit. *J Biol Chem* 287:41560–41568.
33. Papadopoulos S, Leuranguer V, Bannister RA, Beam KG (2004) Mapping sites of potential proximity between the dihydropyridine receptor and RyR1 in muscle using a cyan fluorescent protein-yellow fluorescent protein tandem as a fluorescence resonance energy transfer probe. *J Biol Chem* 279:44046–44056.
34. Eltit JM, et al. (2011) Orthograde dihydropyridine receptor signal regulates ryanodine receptor passive leak. *Proc Natl Acad Sci USA* 108:7046–7051.

Supporting Information

Perni et al. 10.1073/pnas.1716461115

SI Materials and Methods

The expression plasmids for ECFP- and EYFP- $\text{Ca}_v1.1$ (1), EYFP- $\text{Ca}_v1.2$, Stac3-YFP, and unlabeled $\beta1a$ (2), and ECFP- and EYFP-RyR1 (3) were described earlier. EYFP- $\text{Ca}_v1.1$ -N617D was created from EYFP- $\text{Ca}_v1.1$ by using quick-change mutagenesis with forward primer ACGGGTGAGGACTGGGAC-TCCGTGATGTACAAC and reverse primer GTTGTACATC-ACGGAGTCCCAGTCTCACCCGT. To produce a hygromycin-selectable RyR1 construct ("RyR1-pCEP4"), the RyR1 coding sequence was excised with HindIII and MfeI from ECFP-RyR1 and inserted into the multiple cloning sites of the pCEP4 plasmid (Invitrogen). mCherry- $\text{Ca}_v1.2$ was created by replacing the EYFP sequence in YFP- $\text{Ca}_v1.2$ with mCherry from pmCherry-C1 (Clontech) using NheI and HindIII. Stac3-tagRFP was

obtained by using BamHI and NotI to replace EYFP in the Stac3-YFP plasmid with tagRFP from pTagRFP-N (Evrogen). Human JP2 inserted into the pcDNA3.1+/C-(K)DYK expression vector was obtained from Genscript. The JP2 sequence from this plasmid was excised with HindIII and XbaI and substituted for the RyR1 sequence, removed with the same enzymes from EYFP-RyR1 or ECFP-RyR1, to produce EYFP-JP2 and ECFP-JP2, respectively. Unlabeled $\alpha2\delta$ -subunit was provided by William A. Sather, University of Colorado, Anschutz Medical Campus, Aurora, CO. $\text{Ca}_v1.2$ -N739D was provided by Symeon Papadopoulos, University of Cologne, Cologne, Germany. The Stac3 cDNA used as the basis for our tagged Stac3 constructs was provided by Eric N. Olson, University of Texas Southwestern Medical Center, Dallas.

1. Papadopoulos S, Leuranguer V, Bannister RA, Beam KG (2004) Mapping sites of potential proximity between the dihydropyridine receptor and RyR1 in muscle using a cyan fluorescent protein-yellow fluorescent protein tandem as a fluorescence resonance energy transfer probe. *J Biol Chem* 279:44046-44056.
2. Polster A, Perni S, Bichraoui H, Beam KG (2015) Stac adaptor proteins regulate trafficking and function of muscle and neuronal L-type Ca^{2+} channels. *Proc Natl Acad Sci USA* 112:602-606.
3. Hanaichi T, et al. (1986) A stable lead by modification of Sato's method. *J Electron Microscop (Tokyo)* 35:304-306.

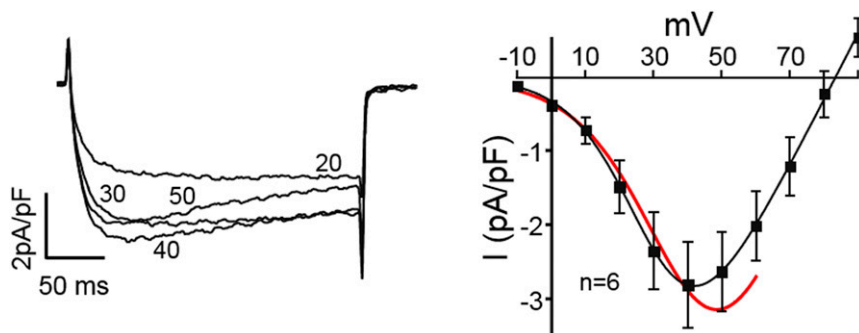


Fig. S1. Representative currents for the indicated test potentials (*Left*) and average peak current vs. voltage relationship (*Right*) measured with the perforated patch technique in tsA201 cells transiently transfected with YFP- $\text{Ca}_v1.1$, $\beta1a$, Stac3-RFP, and JP2 without $\alpha2\delta$. The red curve is replotted from Fig. 2H and corresponds to the peak I - V relationship for cells transfected with YFP- $\text{Ca}_v1.1$, $\beta1a$, Stac3-RFP, and JP2 plus $\alpha2\delta$, measured under slightly different conditions (whole-cell technique, external Ca^{2+} = 10 mM vs. 2.6 mM for the perforated patch technique).

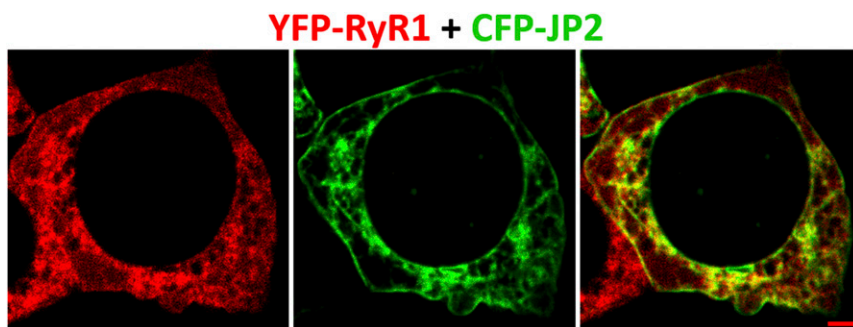


Fig. S2. JP2 alone is sufficient to cause some RyR1 to become associated with the cell surface (tsA201 cell transfected with YFP-RyR1 and CFP-JP2). (Scale bar, 2 μm .)

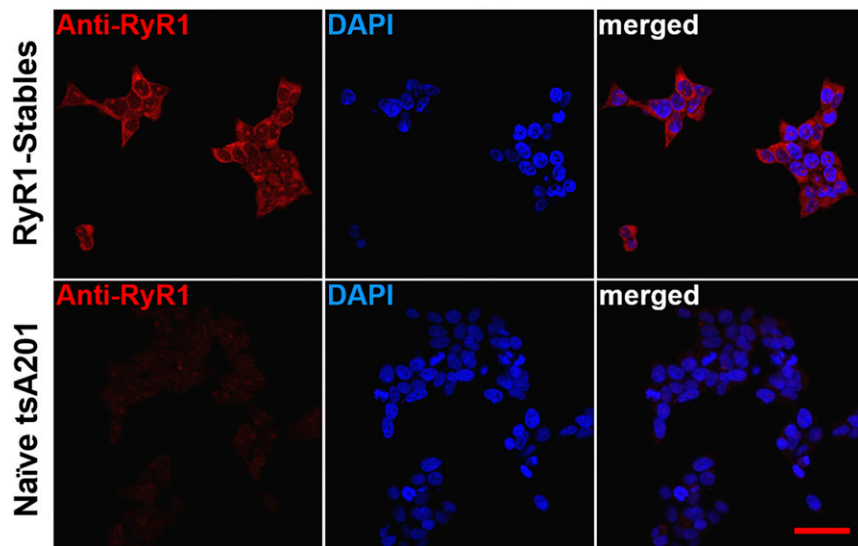


Fig. S3. Immunostaining indicates that RyR1 is expressed in close to 100% of tsA201 cells stably transfected with RyR1 (RyR1-stable cells). With identical immunostaining and image acquisition parameters, little signal was detected in naïve tsA201 cells (*Materials and Methods*). (Scale bar, 50 μm .) Cells were fixed for ≥ 20 min with 4% paraformaldehyde in PBS, washed 3 \times with PBS containing 1% (wt/vol) BSA, and permeabilized/blocked for 1.5 h at room temperature with PBS containing 1% BSA, 10% (vol/vol) goat serum, and 0.5% (wt/vol) Triton X-100. The cells were incubated overnight at 4 $^{\circ}\text{C}$ with monoclonal 34C (Developmental Hybridoma Studies Bank, University of Iowa) diluted 1:50 in PBS/BSA 1%/Triton X-100 0.5%, washed 3 \times , exposed for 1.5 h at room temperature to Alexa 568-conjugated goat anti-mouse (Molecular Probes) 1:1,000 in PBS/BSA 1%/Triton X-100 0.5%, washed 3 \times with PBS, and mounted with DAPI supplemented mounting medium (Vectashield; Vector Laboratories Inc.).

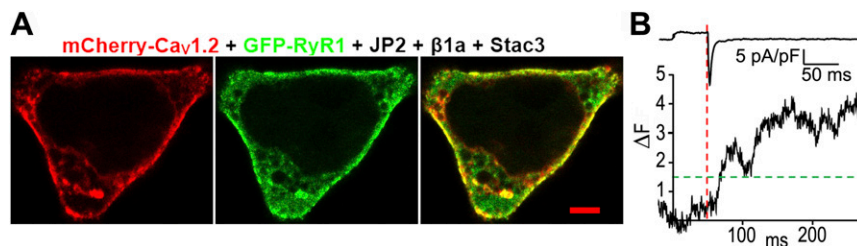


Fig. 54. $\text{Ca}_v1.2$ colocalizes at the surface with RyR1 and supports Ca^{2+} -entry dependent Ca^{2+} transients, in tsA201 cells transfected with constructs for $\text{Ca}_v1.2$, $\beta 1a$, Stac3, JP2, and RyR1. (A) Midlevel confocal section of a tsA201 cell transiently transfected with the indicated constructs. (Scale bar, 5 μm .) (B) Superimposed current (Upper) and Fluo-3 fluorescence change (Lower) in response to a 50-ms step to +90 applied via a perforated patch to an RyR1-stable cell transfected with YFP- $\text{Ca}_v1.2$, $\beta 1a$, Stac3-RFP, and JP2. The red dashed line indicates the time of repolarization to the holding potential (-60 mV). The resulting, large inward tail current triggered a rapid increase in cytoplasmic Ca^{2+} . The green dashed line indicates the threshold ($\Delta F \geq 1.5$ during the 200-ms interval after the onset of depolarization) which was used to determine whether to include fluorescence data for calculation of average responses.

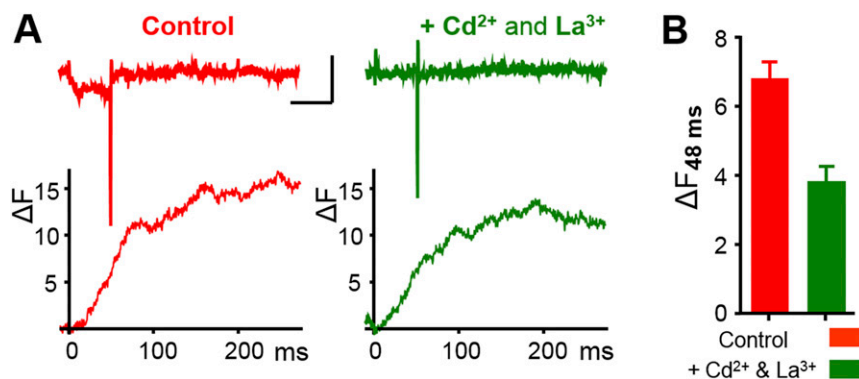


Fig. 55. Depolarization elicits intracellular Ca^{2+} transients that do not require Ca^{2+} entry in RyR1-stable cells transfected with $\text{Ca}_v1.1$, $\beta 1a$, Stac3, and JP2. (A) Ca^{2+} currents (upper traces) and Ca^{2+} transients (lower traces) acquired before and after addition of 0.5 mM Cd^{2+} and 0.1 mM La^{3+} to the solution bathing an RyR1-stable cell transfected with $\text{Ca}_v1.1$, $\beta 1a$, Stac3, and JP2. The cell had been loaded with Fluo-3 AM and was depolarized for 50 ms to +30 mV via a perforated patch. Calibration for the current traces: 2 pA/pF (vertical), 50 ms (horizontal). (B) Average fluorescence change (48 ms after onset of depolarization to +30 mV) measured in five cells (including the one illustrated in A) before (control) and after addition of Cd^{2+} and La^{3+} to the bath. As noted in *Results*, cells not exposed to Cd^{2+} and La^{3+} also produced smaller transients in response to the second of two identical stimuli.

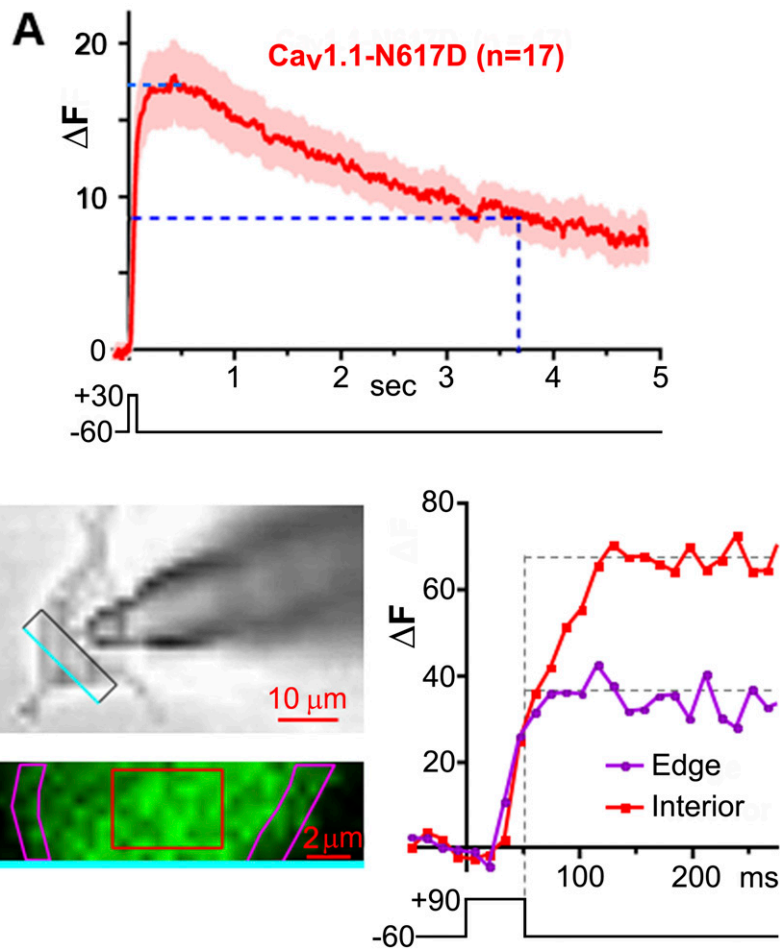


Fig. 56. Calcium removal and release kinetics in tsA201 cells transfected with five triadic proteins. (A) Average change in Fluo-3 fluorescence (\pm SEM) obtained in long-duration recordings of the response to a 50-ms step to +30 applied via a perforated patch to RyR1-stable cells transfected with YFP-Ca_v1.1-N617D, β 1a, Stac3-RFP, and JP2. The fluorescence decayed with a half-time of \sim 3 s, indicating that Ca²⁺ removal processes are slow in these cells. (B) Comparison of fluorescence signals at the edge and interior of an RyR1-stable cell transfected with YFP-Ca_v1.1-N617D, β 1a, Stac3-RFP, and JP2, and depolarized for 50 ms to +90 mV via a perforated patch. Superimposed on the transmitted light image (*Upper Left*) is a rectangle indicating the region subsequently subjected to repetitive confocal scanning (72.7 Hz with each scan lasting 6.87 ms): A single scan obtained \sim 50 ms after repolarization is shown in *Lower Left*. In *Right*, the superimposed dotted lines were drawn by eye to facilitate comparison of the average fluorescence change within the two regions of interest indicated in *Lower Left* (baselines adjusted to be zero before depolarization). The rising phase of the fluorescence increase was more prolonged in the interior than at the edge. Similar results were obtained in a total of five cells, three loaded with Fluo-8 (as for the cell illustrated here) and two with Fluo-3 (which produced smaller and noisier signals).

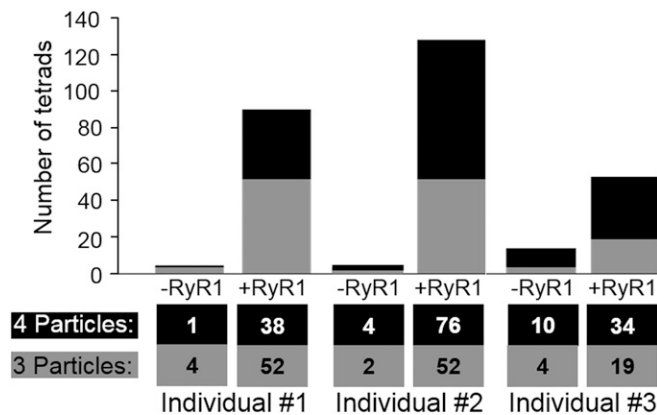


Fig. 57. Numbers of three- or four-particle tetrads as determined by three individuals from freeze-fracture images of naïve tsA201 cells (“-RyR1”) or RyR1-stable cells (“+RyR1”) which had been transfected with YFP-Ca_v1.1, β 1a, Stac3, and JP2. The three individuals were provided 20 unidentified micrographs, 10 each from transfected naïve and RyR1-stable cells, which had similar densities of large particles (1,055 and 1,153 particles per μ m², respectively). The individuals were not informed about how many different conditions were represented.

